

Early season weed mapping in rice crops using multi-spectral UAV data

Daniela Stroppiana, Paolo Villa, Giovanna Sona, Giulia Ronchetti, Gabriele Candiani, Monica Pepe, Lorenzo Busetto, Mauro Migliazzi & Mirco Boschetti

To cite this article: Daniela Stroppiana, Paolo Villa, Giovanna Sona, Giulia Ronchetti, Gabriele Candiani, Monica Pepe, Lorenzo Busetto, Mauro Migliazzi & Mirco Boschetti (2018) Early season weed mapping in rice crops using multi-spectral UAV data, International Journal of Remote Sensing, 39:15-16, 5432-5452, DOI: [10.1080/01431161.2018.1441569](https://doi.org/10.1080/01431161.2018.1441569)

To link to this article: <https://doi.org/10.1080/01431161.2018.1441569>



Published online: 21 Feb 2018.



Submit your article to this journal [↗](#)



Article views: 439








View Crossmark data [↗](#)



Citing articles: 3 View citing articles [↗](#)



Early season weed mapping in rice crops using multi-spectral UAV data

Daniela Stroppiana ^a, Paolo Villa ^a, Giovanna Sona^b, Giulia Ronchetti^b,
Gabriele Candiani ^a, Monica Pepe^a, Lorenzo Busetto ^a, Mauro Migliuzzi^c
and Mirco Boschetti ^a

^aInstitute for Electromagnetic Sensing of the Environment (IREA), Consiglio Nazionale delle Ricerche, Milano, Italy; ^bDepartment of Civil and Environmental Engineering (DICA), Politecnico di Milano, Milano, Italy; ^cWesii Srl, Chiavari, Italy

ABSTRACT

In this article, we propose an automatic procedure for classification of UAV imagery to map weed presence in rice paddies at early stages of the growing cycle. The objective was to produce a weed map (common weeds and cover crop remnants) to support variable rate technologies for site-specific weed management. A multi-spectral orthomosaic, derived from images acquired by a Parrot Sequoia sensor mounted on a quadcopter, was classified through an unsupervised clustering algorithm; cluster labelling into ‘weed’/‘no weed’ classes was achieved using geo-referenced observations. We tested the best set of input features among spectral bands, spectral indices and textural metrics. Weed mapping performance was assessed by calculating overall accuracy (OA) and, for the weed class, omission (OE) and commission errors (CE). Classification results were assessed under an ‘alarmist’ approach in order to minimise the chance of overestimating weed coverage. Under this condition, we found that best results are provided by a set of spectral indices (OA = 96.5%, weed CE = 2.0%). The output weed map was aggregated to a grid layer of 5 × 5 m to simulate variable rate management units; a weed threshold was applied to identify the portion of the field to be subject to treatment with herbicides. Ancillary information on weed and crop conditions were derived over the grid cells to support precision agronomic management of rice crops at the early stage of growth.

ARTICLE HISTORY

Received 31 October 2017

Accepted 5 February 2018

1. Introduction

Within the more general term of precision agriculture, precision agronomy is defined as ‘the matching of agronomic inputs and practices to localized conditions within a field and the improvement of the accuracy of the application’ (Finch, Samuel, and Lane 2014). Benefits of precision agronomy are both financial (saving costs of production) and environmental (reduced risk of pollution) (Finch, Samuel, and Lane 2014; McBratney, Whelan, and Ancev 2005). Technology has a key role in precision agronomy, from data collection, analysis, and interpretation to decision-making and implementation. In

CONTACT Daniela Stroppiana  stroppiana.d@irea.cnr.it  Institute for Electromagnetic Sensing of the Environment (IREA), Consiglio Nazionale delle Ricerche (CNR), Via E. Bassini 15, 20133 Milano, Italy

© 2018 Informa UK Limited, trading as Taylor & Francis Group

particular, remote sensing (RS) techniques are suitable for the assessment of crop status relying on the relationship between canopy/plant optical properties and biophysical parameters, as theoretically shown since early case studies (e.g. Gausman 1973; Peynado et al. 1980; Tucker et al. 1980). Among the advantages of RS are the synoptic view and the reduced cost per unit of area covered (Matese et al. 2015). Although high-altitude RS platforms (i.e. space-borne and air-borne) have been the major source of observations for the optical properties of vegetation (e.g. Eerens et al. 2014; Pan et al. 2015), there have inherent limitations for precision agronomy applications, such as timeliness of the acquisitions, frequency, and spatial resolution (Pinter et al. 2003).

These considerations, together with recent advancements in micro-technologies, have significantly pushed forward the use of Unmanned Aerial Vehicles (UAVs) for crop monitoring; these low-altitude systems can be complementary to high-altitude systems or even an alternative source of information over small areas (Huang et al. 2013). Compared to high-altitude platforms, UAVs offer several advantages, such as: i) the ultra-high spatial resolution, with pixel size of few cm, ii) less limitations imposed by weather conditions, since they can fly also on cloudy days, iii) greater flexibility in acquisition scheduling and payload options, and iv) reduced costs of vehicles and sensors (Torres-Sánchez et al. 2014; Xiang and Tian 2011). Recent review articles published by Salamí, Barrado, and Pastor (2014) and Pádua et al. (2017) well summarize potentials and applications for new generation UAV platforms.

During the last few years, scientific literature on the topic of precision agriculture has been focusing on investigating UAVs capabilities in providing information on: crop status and vigour, stress and disease conditions (e.g. Zarco-Tejada, González-Dugo, and Berni 2012), crop bio-physical parameters (e.g. canopy cover, Leaf Area Index, chlorophyll and nitrogen content; Torres-Sánchez et al. 2014), or potential yield (e.g. Stroppiana et al. 2015). This is particularly relevant for the early stages of crop growth, when fertilizers and herbicides are to be applied and young plants are more sensitive to stress factors, such as diseases and weeds (Mo et al. 2005; Peña et al. 2013; Torres-Sánchez et al. 2014).

UAV imagery were successfully used for mapping weed infestation over maize and sunflower crops (Peña et al. 2013; Pérez-Ortiz et al. 2015; López-Granados et al. 2016; Pérez-Ortiz et al. 2016; Castaldi et al. 2017), as well as grasslands (Tamouridou et al. 2017). In rice crops, UAV data have been exploited for a range of applications, from estimating chlorophyll density and nitrogen content (Uto et al. 2013; Li et al. 2015; Zheng et al. 2016), to assessing lodging (Yang et al. 2017) and mapping yield (Stroppiana et al. 2015; Kim et al. 2017).

Italy is the largest producer of rice in Europe, with about 210,000 ha cultivated area adding up to more than half the EU production (FAO, 2004). Estimated costs for irrigation, seeding, fertilization and crop protection amount to about 35% ($\sim 1000 \text{ € ha}^{-1}$) of the total production costs, with high impact from fertilizers ($\sim 390 \text{ € ha}^{-1}$) and herbicides ($\sim 270 \text{ € ha}^{-1}$) (Camera di Commercio Vercelli 2016). Due to international competition, the European rice production system has to reduce production costs to remain economically sustainable and effective implementation of precision agronomy is the only feasible solution to both reduce costs and environmental impact.

In this framework, our work focuses on testing the capabilities of UAV data in providing information on rice crop status at the early stage of the growth cycle, in order to support the implementation of variable rate technology (VRT) in precision agronomy. The

objective is to characterize the intra-field variability of rice/soil and weed patches from multi-spectral ortho-mosaic imagery acquired with an UAV. In particular, the main goals are: 1) to map non-rice species for site specific weed management, identifying the best performing set of input features in an unsupervised classification approach; 2) to characterize spatial patterns of rice germination to support fertilization strategy; 3) to provide high level information suitable to support VRT applications.

2. Study area

The field object of this study is located in Northern Italy, Pavia province, as illustrated in [Figure 1](#). The field (~ 2 ha) was sown with rice (*Oryza sativa* L., cultivar: Sole CL) on 8 May 2016, with direct machine seeding on dry terrain (row spacing about 10 cm). During preceding winter season, rapeseed (*Brassica napus* L., 1753) was grown as cover crop. The use of cover crops rather than leaving bare fields during autumn/winter is a mean for ecological intensification of arable systems aiming at enhancing productivity by reducing the impact of anthropogenic inputs (Wittwer et al. 2017).

On the date of UAV survey, rice plants in the field were still at very early growth stage (10–15 cm plant height as measured in the field), with a large presence of weeds. Two major weeds were observed in the field: barnyard grass (*Echinochloa* spp.) and common purslane (*Portulaca oleracea* L.); in addition, some rapeseed patches, left from the winter cover crop, were present ([Figure 2](#)). In our study, we define as ‘weed’ all non-rice species which could cause an economic damage by reducing rice production and/or increasing farmer’s production costs and, as a consequence, environmental impact. In this context

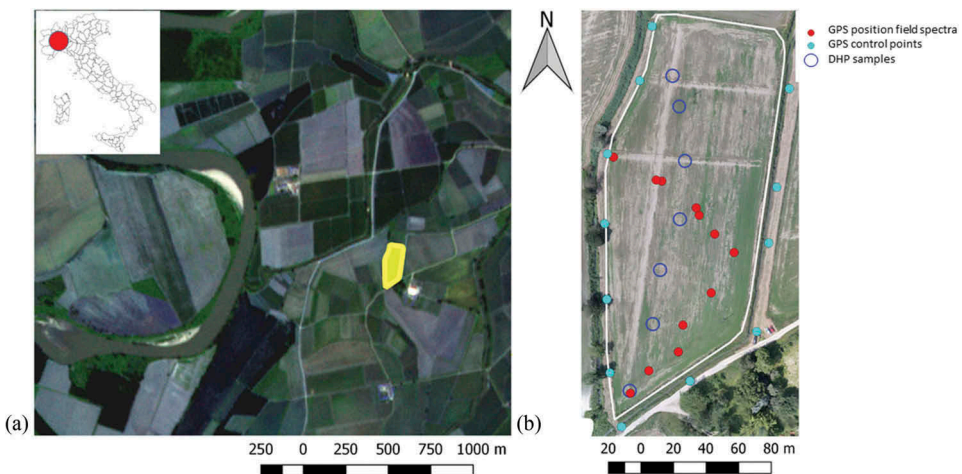


Figure 1. Study area overview: (a) location of the investigated rice field belonging to the Carlo Franchino farm (Rosasco, Lombardy region, Italy) where the experimental flight was carried out on 7 June 2016, overlaid on a true colour composite RapidEye image acquired on 6 June 2016; (b) zoom over the investigated field and the points of crop/weeds *in situ* observations (red circle), hemispherical photos (blue hollow) and GPS reference points (cyan).



Figure 2. Context and detail photos of the rice field object of this study: (a) general conditions, with rapeseed bushes distributed over the field area; (b) barnyard grass weed; (c) zoom over rapeseed plant; (d) common purslane weed.

‘weed’ is used as synonymous of ‘invasive/noxious’ in contrast with ‘alien’ species, which indicate non-indigenous or exotic species (Ziska et al. 2011).

3. Dataset

3.1. *In situ* data

In situ observations and measurements were collected along a transect of points within the monitored rice field on 7 June 2016, simultaneously to UAV overflight. The location of the points of *in situ* data is shown in Figure 1(b).

Vegetation characteristics of either rice or weeds and their conditions were observed and photographed at each point location; for rice only, plant height was also measured. At the same point locations, spectral response was collected with a SR-3500 High Resolution Full Range Lab Spectroradiometer (350–2500 nm) equipped with a 25° fiber optic. The instrument has a variable spectral resolution (3 nm from 350 to 1000 nm, 8 nm from 1000 to 1900 nm, 6 nm from 1900 to 2500 nm) and a sampling interval of 1 nm. Spectra were taken at about 1.50 m above the target, resulting in an optical field-of-view of 1.5–1.7 m² (circular area); each spectrum was recorded as average of 10 measurements. A total of 12 sites were sampled, covered by rice, weeds, and soil with different proportions (Figure S1). Reference spectra of portable Spectralon panel were taken alongside vegetation spectra for converting the spectra samples into reflectance units.

GPS coordinates were determined in correspondence of the signature data positions, by GPS receiver (Topcon HyperPro L1/L2) in network real time kinematic (NRTK) mode, with network corrections provided by NetGeo. The same instrument was used for surveying 12 Ground Control Points (GCPs), pre-signalized with black and white panels along the edges of the field, aimed at an optimal photogrammetric processing of the aerial images taken from the UAV. GCPs coordinates are determined with a precision of 2 cm in planimetry and 3 cm in altimetry. Field measurements and observations are summarized in Supplementary Materials (Figure S1).

Furthermore, digital hemispherical photos (DHPs) were taken in seven different locations across the field, where weed presence was not prevalent over rice (Figure 1(b)). At each site, eight photos were shot from nadir at different azimuth angles, pointing the camera downwards at around 1.30 m from the surface using a NIKON D5200 equipped with a SIGMA 4.5 mm Circular Fisheye lens. DHPs were subsequently processed using CAN-EYE software (v6.1) for deriving rice fractional cover ($f_{C_{rice}}$) according to the methods described by Jonckheere et al. (2004) and Weiss et al. (2004), roughly corresponding to vegetation conditions of the circular area around each sampling site (~7.5 m diameter).

3.2. UAV imagery

UAV imagery were acquired on 7 June 2016 about one month after rice sowing. UAV flight was conducted between 14:00 and 16:00 local time with the 3DRobotics SOLO quadcopter drone mounting a Parrot Sequoia multi-spectral sensor.

Image frames along the flight path were acquired at 70 m above ground level (AGL) with longitudinal and transversal overlaps both equal to 90%, leading to a ground sampling distance (GSD) of 5 cm (Figure 3). In total, 393 frames were acquired to cover the investigated area, and, after visual inspection, 340 were retained for producing the ortho-mosaic.

The Parrot Sequoia multi-spectral sensor acquires imagery through five separate optics: one RGB sensor and four separated sensors for single spectral bands acquisition, namely (central wavelength): green (550 nm), red (660 nm), red-edge (735 nm) and near-infrared (790 nm). With the exception of red-edge, characterized by a 15 nm full width at half maximum (FWHM), all other spectral bands are characterized by FWHM of about 40 nm. On

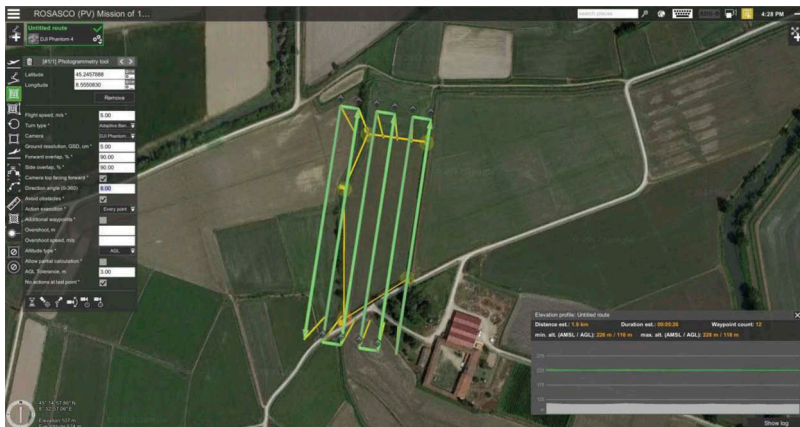


Figure 3. The flight plan for the UAV survey over the investigate rice field.

the Parrot Sequoia, an up-ward facing Sunshine sensor is also available to measure the irradiance for an automatic calibration of multi-spectral images. Unfortunately, due to the Sunshine malfunction, no irradiance measurements were collected during the flight.

3.3. Reference dataset

The reference dataset is composed of points, labelled as 'weed' and 'no weed', used for labelling and validation (i.e. accuracy assessment) of the classification outputs. The approach proposed by Olofsson et al. (2014) was applied to assess the total number of points to be sampled for computing the confusion matrix (n_{TOT}). Following authors equation (13) and assuming i) uniform distribution of the 'weed' and 'no weed' classes, ii) expected user's accuracy for both classes around 80% and iii) estimation error of OA around 2%, we obtained $n_{TOT} = 400$. The same cardinality was chosen for the set of points used for labelling. Therefore, a total of 800 points were extracted with a random

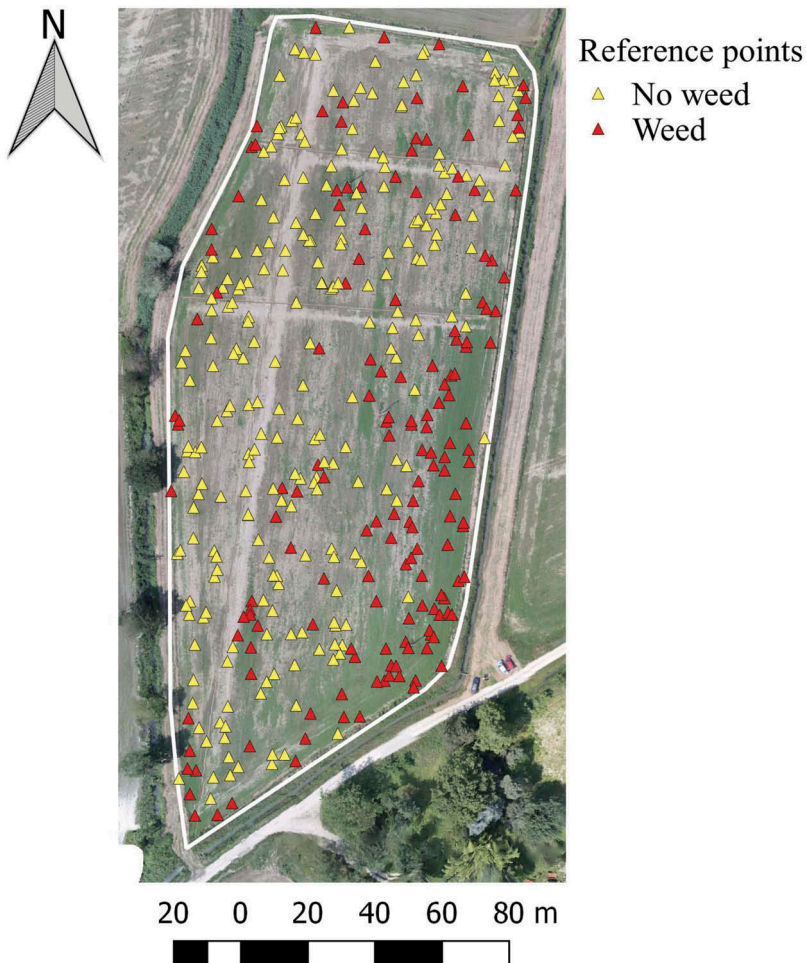


Figure 4. The spatial distribution of the reference points over the field under investigation.

sampling scheme over the field extent and assigned to either 'weed' or 'no weed' class (Figure 4). Class assignment was performed by photo-interpretation of the multi-spectral ortho-mosaic, with the assistance of context photos taken in the field. A total of 315 (485) points were labelled as 'weed' ('no weed') and randomly split into labelling (157 'weed', 243 'no weed') and validation (158 'weed', 242 'no weed') sets.

4. Methods

4.1. Image mosaicking

The Sequoia acquisition produced two kinds of data set simultaneously: a block of RGB images, and a block of multi-spectral images (4 bands). Due to the difference in quality and resolutions of the sensors, the two blocks were independently oriented with Pix4Dmapper (v3.1.23), exploiting the GCPs, surveyed with GPS.

Both RGB and multi-spectral blocks were oriented with a self-calibration processing. Then, according to a consolidate procedure (Sona et al. 2014), two Digital Surface Models (DSMs) were created by using the two oriented blocks of images, with a ground resolution of 0.30 m, and RGB and multispectral ortho-mosaics were produced with resolution of 0.07 m.

4.2. Radiometric calibration

Due to the malfunction of the Sunshine sensor, *in situ* spectral reflectance collected simultaneously with the flight were used for radiometrically calibrating Sequoia bands Digital Numbers (DNs), in an empirical line correction approach (Smith and Milton 1999). First, *in situ* spectra ($n = 12$) were resampled to match the Sequoia bandwidths, whereas DN values were extracted from Sequoia ortho-mosaic spectral bands, over circular areas of 40 cm diameter around each sampling point. Then, linear regression coefficients of DN values against target surface reflectance were calculated.

Radiometric calibration was performed by applying linear regression coefficients to Sequoia spectral bands. Finally, Mean Absolute Error (MAE) and the coefficient of determination (R^2) were calculated for each band. Empirical regression models for the Sequoia spectral bands are shown in Supplementary Materials (Figure S2).

4.3. Spectral indices and textural features calculation

Radiometrically corrected Sequoia band data were used for calculating Spectral Indices (SIs), commonly used as proxy of vegetation parameters. A set of 15 indices was computed; the full list of indices and references are given in Supplementary Materials (Table S1). From this list, a subset of five indices was selected, representing different categories, including: i) a general, well-known index of vegetation vigour and cover (NDVI; Rouse et al. 1974); ii) soil background-adjusted index (SAVI; Huete 1988); iii) a simple ratio index related to leaf pigments content and greenness (RGRI; Gamon and Surfus 1999); iv) an index using the information provided by reflectance in the red edge region, connected to chlorophyll content and leaf area index (NDRE; Barnes et al. 2000);

and v) an index combining visible and near-infrared (NIR) spectral ranges for estimating canopy chlorophyll content (CVI; Hunt et al. 2011).

Together with spectral features, some textural features, based on co-occurrence filters, were computed to highlight spatial patterns of the multi-spectral ortho-mosaic. Textural features are among the most used features in remote sensing classification (Haralick, Shanmugam, and Dinstein 1973; Su and Gibeaut 2017), allowing for the representation of spatial patterns of an image. Some recent works reported a significant improvement of classification accuracy of very high-resolution (VHR) data when these features are combined with spectral features (Qin 2015). Using ITT HARRIS ENVI® (v5.4), five textural features, along the vertical, horizontal and diagonal directions, were computed from the multi-spectral ortho-mosaic: variance, homogeneity, contrast, dissimilarity, and entropy. Each parameter was averaged over the selected directions. An additional set of textural features was derived by computing features over one single direction (horizontal) and by adding three further features (namely mean, second moment and correlation). Accuracy of unsupervised classification has been proved to slightly change with window size used for the computation of textural features and generally decreases with increasing sizes: based on Su and Gibeaut (2017), who investigated the accuracy of classification of UAV imagery with variables window size, a 3 by 3 pixels (pixel size = 0.07 m) window was selected. Furthermore, a Principal Component Analysis (PCA) was run to reduce the dimensionality of input textural features space, i.e. using different subsets of principal components (PCs) as input of the unsupervised classification.

4.4. Weed classification

Radiometrically-corrected data were processed to produce maps of weed/no weed presence, at the spatial resolution of the UAV multi-spectral ortho-mosaic. [Figure 5](#) shows the flowchart of the processing steps, which are described in details in the following paragraphs.

4.4.1. Testing of input features

Spectral and textural features were used as input to the unsupervised classification algorithm to the aim of investigating the influence of input features characteristics on the accuracy of the weed map. [Table 1](#) summarizes the sets of input features used.

4.4.2. Unsupervised classification and automatic labelling

A pixel-based unsupervised ISODATA (Interactive Self-Organizing Data Analysis Technique) algorithm, implemented in the software ITT HARRIS ENVI® (v5.4), was applied to classify image pixels into clusters, i.e. aggregation of pixels in the multi-dimensional space of the input features (Jain, Murty, and Flynn 1999; Arai and Bu 2007). Among the ISODATA parameters, the range of output classes was set to vary between 5 and 10 in order to allow the algorithm to converge to the optimal number of clusters: this number is adjusted automatically during each iteration by merging similar clusters and splitting clusters with large standard deviations. The number of clusters was selected conservatively higher than the target classes (i.e. binary classification into 'weed' and 'no weed') in order to take into account intra-class variability assuming that similar clusters can be merged at following steps (Richards 2013). The number of iterations was conservatively set to 100 to assure

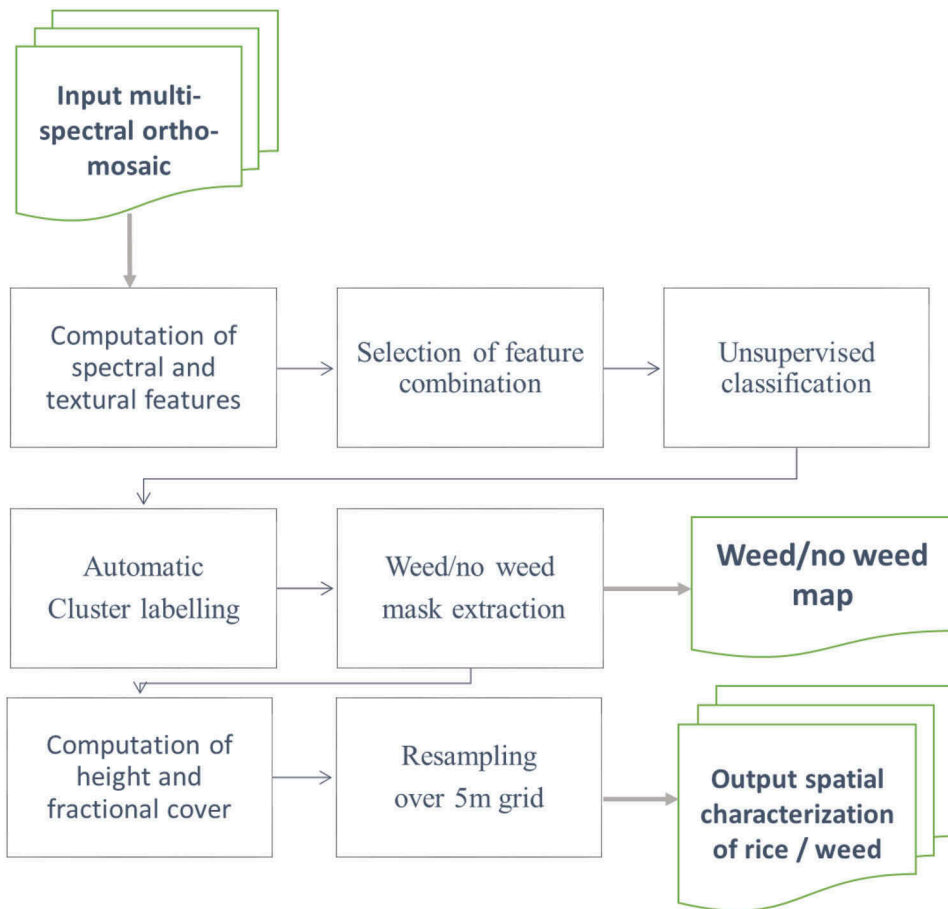


Figure 5. The flowchart of the processing steps applied to derive the weed/no weed maps and ancillary information on rice cover and weed canopy height.

convergence of the algorithm (Broder et al. 2014). A mask over the field perimeter was applied before running the ISODATA algorithm to discard areas outside the field under investigation.

In order to label clusters extracted by the unsupervised algorithm, ISODATA outputs were compared to the labelling subset of reference points ($n = 400$) and each cluster was assigned the 'weed'/'no weed' label based on a majority criterion; a weed/no weed mask is therefore extracted for each unsupervised classification. ISODATA clusters with no reference points were labelled as 'unclassified'.

4.4.3. Classification comparison

The classification outputs derived with the different sets of input features were compared and ranked by using the reference points set aside for validation ($n = 400$), independent from the ones used for labelling of ISODATA clusters. A pixel-based accuracy assessment was applied by comparing pixel by pixel reference and classification datasets.

For each weed map produced, the confusion matrix and global (i.e. overall accuracy) and omission and commission errors for the 'weed' class were computed. The

Table 1. The sets of spectral and textural features used as input to the unsupervised algorithm.

Feature set name	No. of layers	Description
NDVI	1	Only NDVI index
SAVI	1	Only SAVI
GSAVI	1	Only GSAVI
Refl	4	All spectral bands
SIs_all	15	All spectral indices
SIs_subset	5	A subset of spectral indices selected by grouping the indices in categories
Text 1	32	All textural features derived with method 1 (only one direction)
Text1sub	8	A subset of all textural features derived with method 1 (only one direction) selected by the expert
Text1pca02	2	The first 2 components of the PCA applied to the set of textural features derived with method 1
Text1pca03	3	The first 3 components of the PCA applied to the set of textural features derived with method 1
Text1pca04	4	The first 4 components of the PCA applied to the set of textural features derived with method 1
Text1pca05	5	The first 5 components of the PCA applied to the set of textural features derived with method 1
Text1_ind_sub	13	A subset of spectral indices and textural features derived with method 1
Text2	12	All textural features derived with method 2 (three directions)
Text2pca02	2	The first 2 components of the PCA applied to the set of textural features derived with method 2

classification with the best accuracy performance was finally used to derive information on weed presence and density over regular square grid cells of 5 m side, suitable for supporting variable rate technology (VRT) applications.

4.5. Ancillary layers

After the production of the weed/no weed map, ancillary information on rice fractional cover (fC_{rice}) and weed canopy height (cH_{weed}) were produced over the 5 m square grid mentioned above.

4.5.1. Rice fractional cover

The rice fractional cover (fC_{rice}) layer was generated for the area classified as 'no weed' via empirical regression modelling calibrated using *in situ* collected rice fC data. Linear regressive models were fit to the five selected SIs computed from Sequoia data, using as predictive variable the average of each SI over the circular area (~7.5 m diameter) centred at the location of DHPs taken in the field. The model with SAVI as input provided the best results in terms of R^2 (see Supplementary Materials, Table S2 and Figure S3), and was therefore selected for mapping fC_{rice} over the 5 m grid cells, using the following equation:

$$fC_{\text{rice}} = 0.74 (\text{SAVI}) - 0.05 \text{ range } : [0.00 - 0.35] \quad (2)$$

4.5.2. Weed canopy height

The height of weed canopy (cH_{weed}) was estimated by mathematical difference of the multi-spectral DSM and the Digital Terrain Model (DTM). DTM was generated from values of GPS measurements located within the border of the field (red markers in Figure 1). Spatial interpolation was carried out in QGIS (v2.18) by

applying the Triangulated Irregular Networks (TIN) method; output DTM showed values ranging from 152.42 m to 152.52 m, compatible with the expected paddy field elevation. Weed canopy height was calculated by subtracting the DTM from the original DSM. The cH_{weed} layer was derived at the spatial resolution of the DSM (0.30 m) and resampled over the VRT grid (5 m). Since altimetric accuracy of the DMS is around 8 cm and rice plants height in the field was measured to be 10–15 cm, this procedure was retained only to assign canopy height to weed patches, which showed higher top of canopy levels, possibly surpassing 30 cm.

5. Results

5.1. Image pre-processing

Figure 6 shows the output of the pre-processing of Sequoia imagery: false colour composite of the multi-spectral ortho-mosaic (RGB: NIR, red, green) (a), the RGB camera ortho-mosaic (b) and the Digital Surface Model (DSM) (c). All images highlight the presence of weeds, mostly common purslane (*Portulaca oleracea L.*), in the lower right corner of the field. In these areas, which are characterized by both higher canopy and greater biomass (shown in the false colour composite) weed species are dominant; over the field rice plants are still at the very early stages of the growing cycle (young shoots with 3–4 leaves, BBCH code = 13–14).

The geometrical quality of photogrammetric processing was evaluated through the accuracies of estimated targets coordinates with respect to the ones surveyed with GPS technique. In Table 2, mean accuracies on 12 GCPs for RGB and multi-spectral processing are reported.

Values showed in Table 2 point out a slightly lower accuracy of multi-spectral block adjustment. This could be attributed to a difference in GCP search procedure.

During the processing of the Sequoia multi-spectral block, the four single channels were not automatically recognized as forming a single multi-band frame, and the 340 multi-spectral images were actually treated as 4×340 separated images. Therefore, the manual procedure of

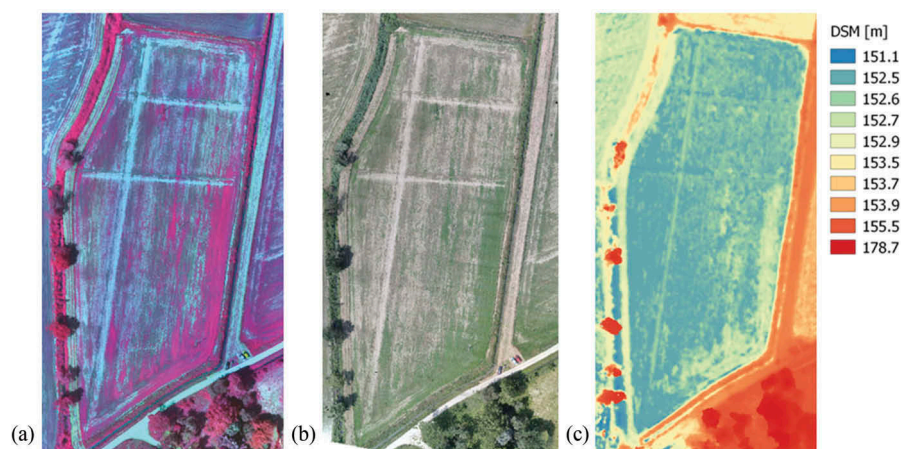


Figure 6. Ortho-mosaics and derived products from UAV data processed with Pix4D: (a) false colour composite (Sequoia NIR-Red-Green multispectral bands displayed in RGB channels); (b) true colour composite from Sequoia RGB camera; (c) Digital Surface Model (DSM).

Table 2. Mean accuracies on ground coordinates of GCPs.

Ortho-mosaic product	X error (m)	Y error (m)	Z error (m)	Total error (m)
Multi-spectral block	0.049	0.058	0.079	0.110
RGB block	0.046	0.033	0.023	0.061

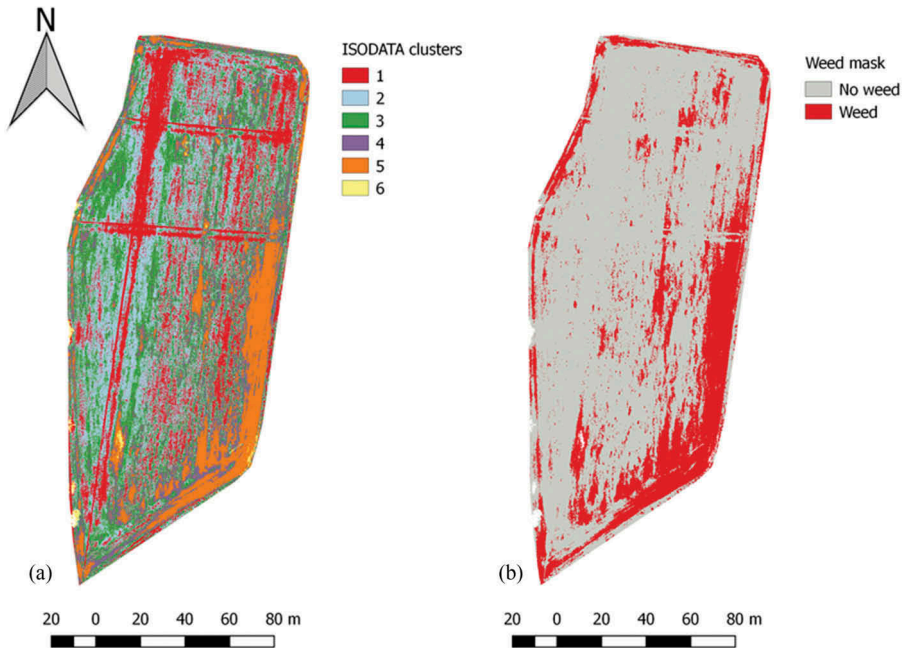


Figure 7. An example of output results from the unsupervised classification flowchart depicted in Figure 5: (a) ISODATA output clusters (six) derived from SIs input set, (b) the weed/no weed mask obtained from automatic labelling.

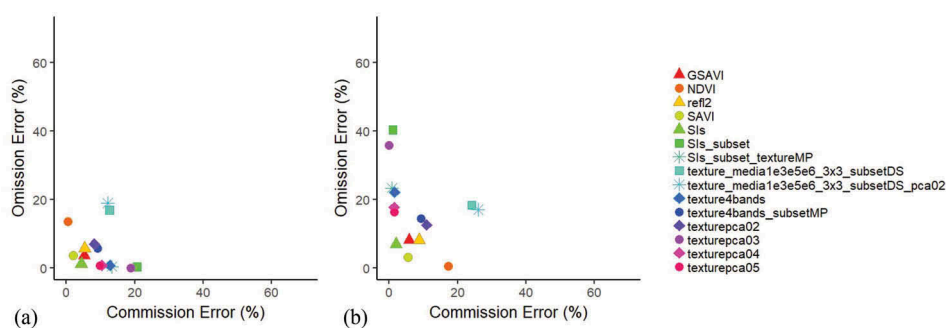
pointing the GCPs on these images had to be repeated separately on all channels and images, thus increasing the error effect of manual pointing. The new releases of Sequoia fixed this problem, and multi-spectral images are now automatically co-registered by Pix4D before the block adjustment. Radiometric calibration performance is deemed enough for the target application, with full details provided as Supplementary Materials (Figure S2).

5.2. Weed classification

Figure 7(a) shows the cluster map derived from ISODATA classification of SIs; the six clusters represent homogeneous areas of the field automatically identified by the unsupervised algorithm. The weed/no weed mask (panel b) is derived by automatic labelling of the ISODATA output as described in 4.4.2. Notice that if no reference points fall into a cluster, pixels are assigned an 'unclassified' label; in the example of Figure 7, this occur for the last cluster (cluster 6, yellow). The total number of output clusters varied as a function of the set of input features as shown in Table 3; weed maps obtained from all input feature sets are presented in Supplementary Material, Figure S4.

Table 3. The Overall Accuracy of the weed/no weed maps obtained from automatic classification of the different input feature sets.

Input feature set	Overall accuracy (%)	No. of layers	No. output clusters (No. labelled)	CE(weed) (%)	OE(weed) (%)
GSAVI	94.5	1	5 (4)	5.8	8.2
NDVI	91.5	1	5 (5)	17.4	0.6
Refl	93.3	4	5 (5)	8.8	8.2
SAVI	96.5	1	5 (5)	5.6	3.2
SIs	96.5	15	6 (5)	2.0	7.0
SIs_subset	83.9	5	5 (3)	1.1	40.4
Text1_ind_sub	90.5	13	7 (6)	0.8	23.4
Text2	82.5	12	5 (5)	24.1	18.4
Text2pca02	81.8	2	5 (5)	26.0	17.1
Text1	90.8	32	10 (9)	1.6	22.2
Text1sub	90.8	8	10 (10)	9.4	14.6
Text1pca02	90.8	2	10 (10)	11.0	12.7
Text1pca03	85.9	3	10 (9)	0.0	35.9
Text1pca04	92.5	4	10 (9)	1.5	17.7
Text1pca05	93.0	5	10 (9)	1.5	16.5

**Figure 8.** The omission and commission errors obtained from the automatic labelling of the ISODATA clusters for the ‘no weed’ (a) and ‘weed’ (b) classes. Each marker represents accuracy metrics for the classified map produced with one specific input feature set.

Overall accuracy (OA) of weed maps obtained from the different sets of input features is given in Table 3; omission (OE) and commission (CE) errors for the ‘weed’ class are shown in Figure 8. The five best performing feature sets, ranked by OA, are: SAVI (96.5%), SIs (96.5%), GSAVI (94.5%), Refl2 (93.3%) and Text1pca04 (92.5%).

The minimization of the commission error over the ‘weed’ class, CE(weed), is assumed as the best criterion to reduce the risk of overestimating weed area, which leads to applying more agrochemicals than needed. Under this assumption, the weed/no weed mask derived by exploiting ‘SIs’ input feature (whole set of 15 spectral indices) is considered the best performing one (CE(weed) = 2.0%, OE(weed) = 7.0%), and is taken for subsequent analyses.

5.3. Products for VRT applications

The weed map derived from ‘SIs’ input feature was resampled to provide the weed cover percent over the 5 m grid layer (Figure 9(a)). In this example, field proportion to be treated

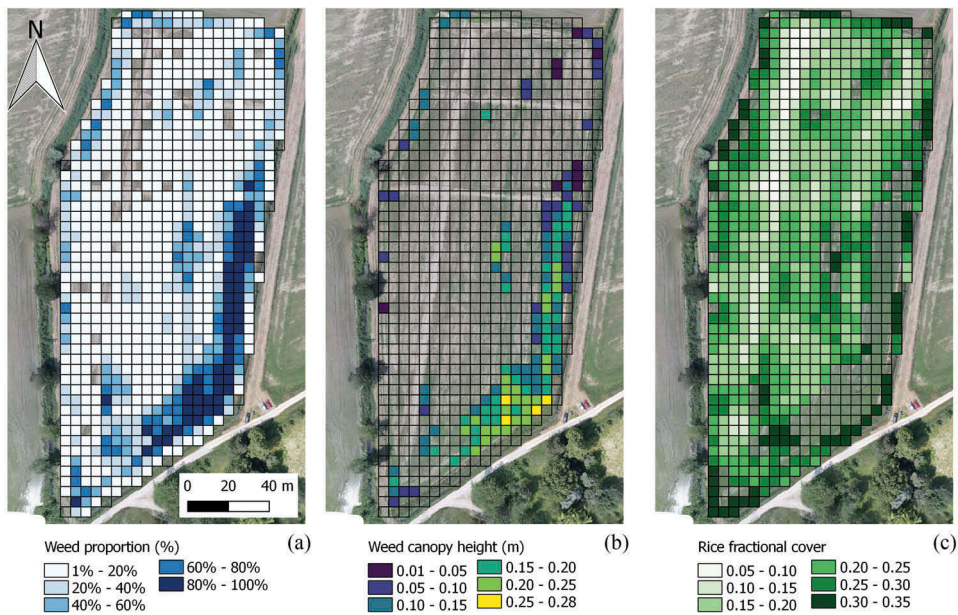


Figure 9. Ancillary VRT information layers produced starting from best performing ‘weed’/‘no weed’ map to support precision agriculture. Information layers are provided over 5 m x 5 m grid cells: (a) weed cover proportion (%), (b) weed canopy height (ch_{weed}) and (c) rice fractional cover (fc_{rice}). Maps are overlaid on RGB colour composite of the UAV ortho-mosaic. Empty cells represent (a) 0% weed cover, (b) weed cover proportion greater than 50% and (c) weed cover proportion less than 50%.

has a maximum value of 95%, when weed threshold is 0% (i.e. all grid cells with a weed proportion greater than 0 are selected). When a weed threshold of 50% is chosen, only grid cells with a majority of weed presence are treated (i.e. approximately 17% of the field area). The ch_{weed} map is provided only over grid cells covered by weeds for more than 50%, as shown in Figure 9(b). In the map, weed canopy height ranges between 0.01 m and little less than 0.30 m. Conversely, fc_{rice} information is meaningful only over cells with prevalence of rice; the example for weed threshold of 50% is shown in Figure 9(c).

6. Discussion

We proposed here a semi-automated procedure for mapping weeds at the early vegetative stages of rice crops. Input to the procedure is the multi-spectral ortho-mosaic of Sequoia spectral bands in the visible to NIR range, at 0.07 m spatial resolution. Imagery planimetric accuracy is in the range 0.05–0.06 m, which was achieved by manual selection of the best frames during photogrammetric processing. Indeed, automatic processing of all Sequoia frames led to lower planimetric accuracy. Accuracy levels are suitable for precision agronomy applications where the management unit that can be handled by VRT machineries is in the best case of few meter size.

Lower spatial resolution (0.30 m) due to spatial filtering, as well as altimetric error of Sequoia ortho-mosaic (around 0.08 m), are to be taken into account when deriving DSM to map canopy height, especially during early stages of the growing season. For our case

study, rice plants are 10–15 cm high while typical height of weeds found in the surveyed field reached up to 30 cm. Therefore, canopy height estimates derived from the elaboration of Sequoia DSM was used only to characterize denser weed patches. This information could be used by the farmer to set the levels of herbicides to be applied in the portions of the field to be treated.

Field spectra were used for empirical calibration of the multi-spectral orthomosaic. The malfunction of the Sunshine sensor did not allow us to investigate the accuracy of the radiometric signal of Sequoia, which should ideally be able to provide radiometrically corrected data. Indeed, the availability of automatically calibrated UAV reflectance images is desirable especially for multi-temporal monitoring and the Sequoia configuration with irradiance sensor is potentially suitable for this purpose.

The approach for weed mapping is based on unsupervised classification and labelling of clusters relying on available geocoded *in situ* observations (i.e. reference points). In this study, the reference dataset was built by random sampling and photo-interpretation of UAV imagery, although any other source of information could be exploited. If *in situ* observations are available to perform the automatic labelling task, the procedure proposed could be automatized. Reference points could be collected with Smart Applications on mobile devices (Bordogna et al. 2016) or provided by volunteers photo-interpreting sample images as demonstrated in numerous open collaborative projects in several fields of science (Franzoni and Saueremann 2014); an example is the Ground Truth 2.0 project, funded by the European Commission, which uses citizen science for land and natural resources management (Ground Truth 2.0 2017).

The output of the proposed procedure is a weed/no weed map at very high spatial resolution, which can be exploited to extract information on weed cover proportion over management units. A weed threshold can be applied to provide treatment maps showing the rice field regions to be treated for weed extirpation. In the weed control decision process, the size of the management unit and the weed threshold can be customized by the user (López-Granados et al. 2016). Based on the mapped field portions to be treated, a set of high-level geo-information layers was derived, namely canopy weed height (cH_{weed}) and rice fractional cover (fC_{rice}), to support decision process in a precision agronomy scenario, i.e. for weed control and rice germination assessment. Weed canopy height could be useful for an approximate estimation of weed volume, which could drive the decision on the amount of herbicide to be applied over those areas of the field where weed species are dominant.

Regarding weed mapping performance, the highest classification accuracy was obtained from spectral features (indices and bands), scoring OA > 91%, with the exception of the 'SIs_subset' input feature set. This demonstrates that spectral information, even when summarized into a single index (NDVI, SAVI, GSAVI) has capability to resolve different vegetation targets, hence maximising the separability between classes (weeds and rice, here). Among the tested spectral indices, GSAVI and SAVI outperformed NDVI in terms of both OA and 'weed' class CE, due to their capacity in dealing with mixed soil/vegetation signal and less sensitive saturation effect over medium to dense canopies. Indeed, at the early stages of the growth cycle, plant density of herbaceous crops is low (estimated fC_{rice} not exceeding 30%) and local variability of soil signal, which

in paddy rice crops is principally due to variability in moisture conditions, can strongly affect spectral measurements.

NDVI is vastly used in precision agriculture for its simplicity (often in absence of a quantitative assessment of the alternatives), but here shows lower OA and a clear tendency to overestimate weed presence, due to the nonlinear relation of the index to crop presence (Table 3). In fact, NDVI is highly sensitive to abrupt changes from bare soil to crop presence when there is a strong contrast between soil and plant in NIR reflectance such as in post emergence phase (Huete 1988; Boschetti 2006). In contrast, soil adjusted SIs (SAVI and GSAVI) provided results more accurate than NDVI when a single index is used for straightforward weed mapping.

The number of output clusters resulting from the best performing sets of input features is in the range 5–6 (Table 3), along the lower bound of clusters' range, thus confirming the robustness of the choice of setting the upper bound of output clusters range equal to 10. The underperformance of SIs_subset, which shows a strongly underestimated weed mask ($OE(\text{weed}) > 40\%$) is connected to the fact that 2 out of 5 ISODATA clusters for this input feature sets were not labelled because no reference point fell in them, leading to size-unbalanced clusters which is not shown by any other tested set.

When textural features are added to spectral information, the number of output clusters increases up to 10, thus suggesting that more variability is observed in the data. However, this heterogeneity does not result into higher accuracy, meaning that information about texture does not bring additional value for the discrimination of rice against weed, at least for the agronomic conditions of the field object of this study (machine-seeded rice over dry terrain, BBCH scale 13–14). Among the textural features, the ones derived taking into account a single shift direction (feature sets with 'Text1' prefix) are more variable in their outcomes – with OA varying from 86% to 93%, depending on number of considered PCAs. However, they are more accurate in distinguishing weeds from no weed, when compared to textural features averaged across the four shift directions (feature sets with Text2 prefix).

The selection of the best performing classification depends on the objectives of the application, in relation to an 'alarmist' (accept the risk of overestimating weed area) or 'precautionary' (accept the risk of missing weed area) attitude. Since we aim at the optimization of the weed treatments by saving input resources and reducing environmental impacts, we privileged the lowest weed overestimation (i.e. weed commission error). Therefore, we selected the weed map derived from SIs feature set (OA = 96.5%, weed CE = 2.0%, weed OE = 7.0%). SAVI and GSAVI, only slightly less accurate in terms of weed mapping, could be a robust alternative to the whole set of SIs if the minimization of input features was a requirement for the optimization of computational costs.

Starting from accurate weed maps it is possible to further exploit the information content of multi-spectral UAV data, i.e. by providing information about weed height and rice fractional cover, which can allow more spatially accurate herbicides distribution and possibly taking measures for adjusting fertilization according to rice germination rate.

7. Conclusions

A semi-automatic procedure based on unsupervised clustering algorithm was designed and applied to multi-spectral ortho-mosaic of UAV Sequoia images acquired over a rice

field to detect weed presence at the early stages of the growing season. Among the input feature sets tested, spectral information showed better accuracy than textural features. Spectral indices were the most suited inputs and, among them, SAVI and GSAVI showed the best results, with OA higher than 94%. The weed map output of the semi-automatic procedure was exploited, together with additional information derived from the same Sequoia dataset, in order to produce geospatial gridded layers including information on weed abundance and rice germination (i.e. fractional cover). This information could be used in support of precision agronomy management of rice fields.

Acknowledgments

This study was founded in the framework of FP7 ERMES project. (<http://www.ermes-fp7space.eu/>) funded by the European Union Seventh Framework Program (FP7/2007-2013) under grant agreement 606983. The authors acknowledge Parrot company which allows for the use of the Sequoia sensor for scientific research. The authors also wish to thank Azienda Agricola Carlo Franchino (Rosasco, Italy), for hosting our field activity and Dr. Ramin Azar for his help in field data collection.

Disclosure statement

No potential conflict of interest was reported by the authors.

Funding

This work was supported by the European Union Seventh Framework Program; [FP7/2007-2013] under grant agreement 606983.

ORCID

Daniela Stroppiana  <http://orcid.org/0000-0002-5619-4305>

Paolo Villa  <http://orcid.org/0000-0002-6952-836X>

Gabriele Candiani  <http://orcid.org/0000-0001-5270-071X>

Lorenzo Busetto  <http://orcid.org/0000-0001-9634-6038>

Mirco Boschetti  <http://orcid.org/0000-0003-2156-4166>

References

- Arai, K., and X. Q. Bu. 2007. "ISODATA Clustering with Parameter (Threshold for Merge and Split) Estimation Based on GA: Genetic Algorithm." *Report Faculty Science Engineering, Saga University* 36 (1): 17–23.
- Bannari, A., D. Morin, F. Bonn, and A. R. Huete. 1995. "A Review of Vegetation Indices." *Remote Sensing Reviews* 13 (1–2): 95–120. doi:10.1080/02757259509532298.
- Barnes, E. M., T. R. Clarke, S. E. Richards, P. D. Colaizzi, J. Haberland, and M. Kostrzewski. 2000. "Coincident Detection of Crop Water Stress, Nitrogen Status and Canopy Density Using Ground Based Multispectral Data." Proceedings of the Fifth International Conference on Precision Agriculture, 1619 vols., edited by Robert, P. C., Rust, R. H., Larson, W. E., Bloomington, Minnesota, July 16–19, 1–15, ASA-CSSA-SSSA, 2000.
- Bordogna, G., T. Kliment, L. Frigerio, P. A. Brivio, A. Crema, D. Stroppiana, M. Boschetti, and S. Sterlacchini. 2016. "Spatial Data Infrastructure Integrating Multisource Heterogeneous

- Geospatial Data and Time Series: A Study Case in Agriculture." *ISPRS International Journal of Geo-Information* 5 (5): 73. doi:10.3390/ijgi5050073.
- Boschetti, M. 2006. "Monitoring cropping system through remote sensing and crop models." PhD dissertation, Università degli Studi di Milano. Facoltà Di Agraria, Dipartimento di Produzione Vegetale Biologia Vegetale e produttività della pianta Coltivata, Ciclo XVIII.
- Broder, A., L. Garcia-Pueyo, V. Josifovski, S. Vassilvitskii, and S. Venkatesan. 2014. "Scalable K-Means by Ranked Retrieval." Proceedings of the 7th ACM international conference on Web search and data mining, 233–242, ACM, New York, NY, February 24–28.
- Broge, N. H., and E. Leblanc. 2001. "Comparing Prediction Power and Stability of Broadband and Hyperspectral Vegetation Indices for Estimation of Green Leaf Area Index and Canopy Chlorophyll Density." *Remote Sensing of Environment* 76 (2): 156–172. doi:10.1016/S0034-4257(00)00197-8.
- Camera di Commercio Vercelli. 2016. "Il bilancio economico dell'azienda Agricola." Accessed 30 October 2017. http://images.vc.camcom.it/f/Varie/74/7446_CCIAAVC_2722017.pdf
- Castaldi, F., F. Pelosi, S. Pascucci, and R. Casa. 2017. "Assessing the Potential of Images from Unmanned Aerial Vehicles (UAV) to Support Herbicide Patch Spraying in Maize." *Precision Agriculture* 18 (1): 76–94. doi:10.1007/s11119-016-9468-3.
- Chen, J. M. 1996. "Evaluation of Vegetation Indices and a Modified Simple Ratio for Boreal Applications." *Canadian Journal of Remote Sensing* 22 (3): 229–242. doi:10.1080/07038992.1996.10855178.
- Eerens, H., D. Haesen, F. Rembold, F. Urbano, C. Tote, and L. Bydekerke. 2014. "Image Time Series Processing for Agriculture Monitoring." *Environmental Modelling & Software* 53: 154–162. doi:10.1016/j.envsoft.2013.10.021.
- Escadafal, R., and A. Huete. 1991. "Improvement in Remote Sensing of Low Vegetation Cover in Arid Regions by Correcting Vegetation Indices for Soil "Noise"." *Comptes Rendus De l'Academie Des Sciences, Serie 2* 312 (11): 1385–1391.
- FAO (Food and Agriculture Organization). 2004. "The International Year of Rice." Accessed 30 October 2017. <http://www.fao.org/rice2004/en/p7.htm>
- Finch, H. J. S., A. M. Samuel, and G. P. F. Lane. 2014. "Precision Farming." *Chap. 10 in Lockhart & Wiseman's Crop Husbandry Including Grassland (Ninth Edition)*, edited by Finch, H. J. S., A. M. Samuel, and G. P. F. Lane, 235–244, ISBN: 978-1-78242-371-3, doi: 10.1533/9781782423928.2.235.
- Franzoni, C., and H. Sauermann. 2014. "Crowd Science: The Organization of Scientific Research in Open Collaborative Projects." *Research Policy* 43(1): 1–20. ISSN 0048-7333. doi:10.1016/j.respol.2013.07.005.
- Gamon, J. A., and J. S. Surfus. 1999. "Assessing Leaf Pigment Content and Activity with a Reflectometer." *The New Phytologist* 143 (1): 105–117. doi:10.1046/j.1469-8137.1999.00424.x.
- Gausman, H. W. 1973. "Reflectance, Transmittance, and Absorptance of Light by Subcellular Particles of Spinach (*Spinacia Oleracea* L.) Leaves." *Agronomy Journal* 65 (4): 551–553. doi:10.2134/agronj1973.00021962006500040008x.
- Gitelson, A., and M. N. Merzlyak. 1994a. "Quantitative Estimation of Chlorophyll-A Using Reflectance Spectra: Experiments with Autumn Chestnut and Maple Leaves." *Journal of Photochemistry and Photobiology B: Biology* 22 (3): 247–252. doi:10.1016/1011-1344(93)06963-4.
- Gitelson, A., and M. N. Merzlyak. 1994b. "Spectral Reflectance Changes Associated with Autumn Senescence of *Aesculus Hippocastanum* L. And *Acer Platanoides* L. Leaves. Spectral Features and Relation to Chlorophyll Estimation." *Journal of Plant Physiology* 143 (3): 286–292. doi:10.1016/S0176-1617(11)81633-0.
- Ground Truth 2.0. 2017. "Land Use Mapper." Accessed 30 October 2017. <http://gt20.eu/land-use-mapper/>
- Haralick, R. M., K. Shanmugam, and I. Dinstein. 1973. "Textural Features for Image Classification." *IEEE Transactions on Systems, Man, and Cybernetics* 6: 610–621. doi:10.1109/TSMC.1973.4309314.
- Huang, Y., S. J. Thomson, W. C. Hoffman, Y. Lan, and B. K. Fritz. 2013. "Development and Prospect of Unmanned Aerial Vehicle Technologies for Agricultural Production Management." *International Journal of Agricultural and Biological Engineering* 6 (3): 1–10.
- Huete, A. R. 1988. "A Soil-Adjusted Vegetation Index (SAVI)." *Remote Sensing of Environment* 25 (3): 295–309. doi:10.1016/0034-4257(88)90106-X.

- Hunt, E. R., C. S. T. Daughtry, J. U. Eitel, and D. S. Long. 2011. "Remote Sensing Leaf Chlorophyll Content Using a Visible Band Index." *Agronomy Journal* 103 (4): 1090–1099. doi:10.2134/agronj2010.0395.
- Jain, A. K., M. N. Murty, and P. J. Flynn. 1999. "Data Clustering: A Review." *ACM Computing Surveys (CSUR)* 31 (3): 264–323. doi:10.1145/331499.331504.
- Jonckheere, I., S. Fleck, K. Nackaerts, B. Muys, P. Coppin, M. Weiss, and F. Baret. 2004. "Review of Methods for in Situ Leaf Area Index Determination: Part I. Theories, Sensors and Hemispherical Photography." *Agricultural and Forest Meteorology* 121 (1): 19–35. doi:10.1016/j.agrformet.2003.08.027.
- Kim, M., J. Ko, S. Jeong, J. M. Yeom, and H. O. Kim. 2017. "Monitoring Canopy Growth and Grain Yield of Paddy Rice in South Korea by Using the GRAMI Model and High Spatial Resolution Imagery." *GIScience & Remote Sensing* 54 (4): 534–551. doi:10.1080/15481603.2017.1291783.
- Li, J., F. Zhang, X. Qian, Y. Zhu, and G. Shen. 2015. "Quantification of Rice Canopy Nitrogen Balance Index with Digital Imagery from Unmanned Aerial Vehicle." *Remote Sensing Letters* 6 (3): 183–189. doi:10.1080/2150704X.2015.1021934.
- López-Granados, F., J. Torres-Sánchez, A. Serrano-Pérez, A. I. De Castro, F. J. Mesas-Carrascosa, and J.-M. Peña. 2016. "Early Season Weed Mapping in Sunflower Using UAV Technology: Variability of Herbicide Treatment Maps against Weed Thresholds." *Precision Agriculture* 17: 183–199. doi:10.1007/s11119-015-9415-8.
- Lymburner, L., P. J. Beggs, and C. R. Jacobson. 2000. "Estimation of Canopy-Average Surface-Specific Leaf Area Using Landsat TM Data." *Photogrammetric Engineering & Remote Sensing* 66 (2): 183–192.
- Matese, A., P. Toscano, S. F. Di Gennaro, L. Genesio, F. P. Vaccari, J. Primicerio, C. Belli, A. Zaldei, R. Bianconi, and B. Gioli. 2015. "Intercomparison of UAV, Aircraft and Satellite Remote Sensing Platforms for Precision Viticulture." *Remote Sensing* 7 (3): 2971–2990. doi:10.3390/rs70302971.
- McBratney, A., B. Whelan, and T. Ancev. 2005. "Future Directions of Precision Agriculture." *Precision Agriculture* 6 (1): 7–23. doi:10.1007/s11119-005-0681-8.
- Mo, X., S. Liu, Z. Lin, Y. Xu, Y. Xiang, and T. R. McVicar. 2005. "Prediction of Crop Yield, Water Consumption and Water Use Efficiency with a SVAT-Crop Growth Model Using Remotely Sensed Data on the North China Plain." *Ecological Modelling* 183 (2): 301–322. doi:10.1016/j.ecolmodel.2004.07.032.
- Olofsson, P., G. M. Foody, M. Herold, S. V. Stehman, C. E. Woodcock, and M. A. Wulder. 2014. "Good Practices for Estimating Area and Assessing Accuracy of Land Change." *Remote Sensing of Environment* 148: 42–57. ISSN 0034-4257. doi:10.1016/j.rse.2014.02.015.
- Pádua, L., J. Vanko, J. Hruška, T. Adão, J. J. Sousa, E. Peres, and R. Morais. 2017. "UAS, Sensors, and Data Processing in Agroforestry: A Review Towards Practical Applications." *International Journal of Remote Sensing* 38 (8–10): 2349–2391.
- Pan, Z., J. Huang, Q. Zhou, L. Wang, Y. Cheng, H. Zhang, G. A. Blackburn, J. Yan, and J. Liu. 2015. "Mapping Crop Phenology Using NDVI Time-Series Derived from HJ-1 A/B Data." *International Journal of Applied Earth Observation and Geoinformation* 34: 188–197. doi:10.1016/j.jag.2014.08.011.
- Peña, J. M., J. Torres-Sánchez, A. I. Castro, M. De, Kelly, and F. López-Granados. 2013. "Weed Mapping in Early-Season Maize Fields Using Object-Based Analysis of Unmanned Aerial Vehicle (UAV) Images." *PLoS One* 8 (10): e77151. doi:10.1371/journal.pone.0077151.
- Pérez-Ortiz, M., J. M. Peña, P. A. Gutiérrez, J. Torres-Sánchez, C. Hervás-Martínez, and F. López-Granados. 2015. "A Semi-Supervised System for Weed Mapping in Sunflower Crops Using Unmanned Aerial Vehicles and A Crop Row Detection Method." *Applied Soft Computing* 37: 533–544. doi:10.1016/j.asoc.2015.08.027.
- Pérez-Ortiz, M., J. M. Peña, P. A. Gutiérrez, J. Torres-Sánchez, C. Hervás-Martínez, and F. López-Granados. 2016. "Selecting Patterns and Features for Between-And Within-Crop-Row Weed Mapping Using UAV-imagery." *Expert Systems with Applications* 47: 85–94. doi:10.1016/j.eswa.2015.10.043.
- Peynado, A., H. W. Gausman, D. E. Escobar, and R. R. Rodriguez. 1980. "Detecting Freeze Damage to Citrus Leaves." *Hortscience* 15: 435.

- Pinter, P. J. Jr., J. L. Hatfield, J. S. Schepers, E. M. Barnes, M. S. Moran, C. S. T. Daughtry, and D. R. Upchurch. 2003. "Remote Sensing for Crop Management." *Photogrammetric Engineering & Remote Sensing* 69 (6): 647–664. doi:10.14358/PERS.69.6.647.
- Qin, R. 2015. "A Mean Shift Vector-Based Shape Feature for Classification of High Spatial Resolution Remotely Sensed Imagery." *IEEE Journal of Selected Topics in Applied Earth Observations and Remote Sensing* 8 (5): 1974–1985. doi:10.1109/JSTARS.2014.2357832.
- Richards, J. A. 2013. *Remote Sensing Digital Image Analysis - An Introduction*. Heidelberg, Germania: Springer-Verlag Berlin Heidelberg. Vol. XIX vols, 494. doi:10.1007/978-3-642-30062-2.
- Rouse, J. W., R. H. Haas, J. A. Schell, and D. W. Deering. 1974. "Monitoring Vegetation Systems in the Great Plains with ERTS." *NASA Special Publication* 309–317.
- Salamí, E., C. Barrado, and E. Pastor. 2014. "UAV Flight Experiments Applied to the Remote Sensing of Vegetated Areas." *Remote Sensing* 6 (11): 11051–11081. doi:10.3390/rs61111051.
- Smith, G. M., and E. J. Milton. 1999. "The Use of the Empirical Line Method to Calibrate Remotely Sensed Data to Reflectance." *International Journal of Remote Sensing* 20 (13): 2653–2662. doi:10.1080/014311699211994.
- Sona, G., L. Pinto, D. Pagliari, and D. Passoni. 2014. "Experimental Analysis of Different Software Packages for Orientation and Digital Surface Modelling from UAV Images." *Earth Science Informatics* 7 (2): 97–107. doi:10.1007/s12145-013-0142-2.
- Stroppiana, D., M. Migliazzi, V. Chiarabini, A. Crema, M. Musanti, C. Franchino, and P. Villa. 2015. "Rice Yield Estimation Using Multispectral Data from UAV: A Preliminary Experiment in Northern Italy." Proceedings of the Geoscience and Remote Sensing Symposium (IGARSS), 4664–4667, The Institute of Electrical and Electronics Engineers, Inc., Milano, 26–31 July.
- Su, L., and J. Gibeaut. 2017. "Using UAS Hyperspatial RGB Imagery for Identifying Beach Zones along the South Texas Coast." *Remote Sensing* 9 (2): 159. doi:10.3390/rs9020159.
- Tamouridou, A. A., T. K. Alexandridis, X. E. Pantazi, A. L. Lagopodi, J. Kashefi, and D. Moshou. 2017. "Evaluation of UAV Imagery for Mapping Silybum Marianum Weed Patches." *International Journal of Remote Sensing* 38 (8–10): 2246–2259.
- Tian, Y. C., Y. Zhu, and W. X. Cao. 2005. "Monitoring Soluble Sugar, Total Nitrogen & Its Ratio in Wheat Leaves with Canopy Spectral Reflectance." *Acta Agronomica Sinica* 31 (3): 355–360.
- Torres-Sánchez, J., J. M. Peña, A. I. De Castro, and F. López-Granados. 2014. "Multi-Temporal Mapping of the Vegetation Fraction in Early-Season Wheat Fields Using Images from UAV." *Computers and Electronics in Agriculture* 103: 104–113. doi:10.1016/j.compag.2014.02.009.
- Tucker, C. J., B. N. Holben, J. H. Elgin Jr, and J. E. McMurtrey III. 1980. "Relationship of Spectral Data to Grain Yield Variation." *Photogrammetry Engineering & Remote Sensing* 46 (5): 657–666.
- Uto, K., H. Seki, G. Saito, and Y. Kosugi. 2013. "Characterization of Rice Paddies by a UAV-mounted Miniature Hyperspectral Sensor System." *IEEE Journal of Selected Topics in Applied Earth Observations and Remote Sensing* 6 (2): 851–860. doi:10.1109/JSTARS.2013.2250921.
- Weiss, M., F. Baret, G. J. Smith, I. Jonckheere, and P. Coppin. 2004. "Review of Methods for in Situ Leaf Area Index (LAI) Determination: Part II. Estimation of LAI, Errors and Sampling." *Agricultural and Forest Meteorology* 121 (1): 37–53. doi:10.1016/j.agrformet.2003.08.001.
- Wittwer, R. A., B. Dorn, W. Jossi, and M. G. A. van der Heijden. 2017. "Cover Crops Support Ecological Intensification of Arable Cropping Systems." *Scientific Reports* 7: 41911. doi:10.1038/srep41911.
- Xiang, H., and L. Tian. 2011. "Development of a Low-Cost Agricultural Remote Sensing System Based on an Autonomous Unmanned Aerial Vehicle (UAV)." *Biosystems Engineering* 108 (2): 174–190. doi:10.1016/j.biosystemseng.2010.11.010.

- Yang, M. D., K. S. Huang, Y. H. Kuo, H. P. Tsai, and L. M. Lin. 2017. "Spatial and Spectral Hybrid Image Classification for Rice Lodging Assessment through UAV Imagery." *Remote Sensing* 9 (6): 583. doi:[10.3390/rs9060583](https://doi.org/10.3390/rs9060583).
- Zarco-Tejada, P. J., V. González-Dugo, and J. A. Berni. 2012. "Fluorescence, Temperature and Narrow-Band Indices Acquired from a UAV Platform for Water Stress Detection Using a Micro- Hyperspectral Imager and a Thermal Camera." *Remote Sensing of Environment* 117: 322–337. doi:[10.1016/j.rse.2011.10.007](https://doi.org/10.1016/j.rse.2011.10.007).
- Zheng, H., X. Zhou, T. Cheng, X. Yao, Y. Tian, W. Cao, and Y. Zhu 2016. "Evaluation of a UAV-based Hyperspectral Frame Camera for Monitoring the Leaf Nitrogen Concentration in Rice." In *Geoscience and Remote Sensing Symposium (IGARSS), 2016 IEEE International*, 7350–7353. The Institute of Electrical and Electronics Engineers, Inc., July.
- Ziska, L. H., D. M. Blumenthal, G. B. Runion, E. R. Hunt Jr, and H. Diaz-Soltero. 2011. "Invasive Species and Climate Change: An Agronomic Perspective." *Climatic Change* 105 (1–2): 13–42. doi:[10.1007/s10584-010-9879-5](https://doi.org/10.1007/s10584-010-9879-5).